Journal of The Electrochemical Society, **157** (4) H459-H462 (2010)
0013-4651/2010/157(4)/H459/4/$28.00 © The Electrochemical Society

On an AlGaInP Multiple Quantum Well Light Emitting Diode with a Thin Carbon-Doped GaP Contact Layer Structure

Tsung-Yuan Tsai, Yi-Jung Liu, Chih-Hung Yen, and Wen-Chau Liu[z]

Department of Electrical Engineering, Institute of Microelectronics, National Cheng-Kung University, Tainan 70101, Taiwan

An interesting AlGaInP multiple quantum well light emitting diode (LED) with a thin carbon-doped (C-doped) GaP contact layer and a transparent conducting indium tin oxide (ITO) film is fabricated. Moreover, LEDs with different contact layer structures are presented and compared in this work. The experimental results illustrate that the LED with a C-doped GaP contact layer exhibits a higher output power of 31.4 mW and a higher external quantum efficiency of 9%. The light output power, under dc 20 mA operation, of this LED is increased by a factor of 18% compared with conventional LEDs without the C-doped contact and ITO spreading layers. These results are mainly attributed to the improved contact property and lower optical absorption effect. In addition, the studied device shows the lower dynamic resistance (5.1 Ω @ 20 mA), reduced leakage current (1.5×10^{-9} A @ −5 V), reduced wavelength shift (with 1.7 nm variation between 10 and 200 mA), and lower thermal-induced optical degradation (<0.3% during 50 mA, 220 h aging test). Therefore, the studied device shows promise in fabricating high performance AlGaInP LEDs.
 [DOI: 10.1149/1.3314338]

Manuscript submitted November 27, 2009; revised manuscript received January 14, 2010. Published February 25, 2010.

Recently, high brightness visible light emitting diodes (LEDs) have attracted great interest for various applications.[1,2] The quaternary $(Al_xGa_{1-x})_{0.5}In_{0.5}P$ alloy material system, lattice-matched to the GaAs substrates, has a wide bandgap direct transition corresponding to the spectrum region from green ($x = 0.53$, $E_g = 2.3$ eV) to red ($x = 0$, $E_g = 1.85$ eV). Over the past few years, several efforts have been employed to improve the brightness of $(Al_xGa_{1-x})_{0.5}In_{0.5}P$-based LEDs.[3-8] A current approach used in commercially available AlGaInP LEDs is the use of a thick p-type window layer. Generally, GaP [3,4] and AlGaAs [5] were widely employed as window layer materials for current spreading due to their excellent performance of light transparency and uniform carrier distribution. However, the used thick window layer for current spreading increases the production cost.

An indium tin oxide (ITO) layer with high conductance ($\rho = 2.5 \times 10^{-4}$ Ω cm) and superior transparency (>90%) has been introduced to enhance current spreading in AlGaInP-based LEDs.[6-8] However, it is inevitable to increase the turn-on voltage (V_f) due to the poor ohmic contact between the ITO and the window layer.[9] This high contact resistance certainly yields the degradation of electrical characteristics of AlGaInP-based LEDs. Hence, a high doping GaAs contact layer was applied to form an ohmic contact with the ITO film.[6-8] The major disadvantage of this structure, arising from the GaAs contact layer, is the decreased intensity of emitted light due to its absorption characteristics.[9] Recently, an interesting and alternative structure of a high doping GaP contact layer was reported by our group.[10] It was applied to diminish the light absorption and thus increase the light output power of the ITO-assisted LEDs. Some initial results of this AlGaInP-based LED were studied. In this work, the related electrical and optical properties are further investigated in detail.

Experimental

The epitaxial layers of studied AlGaInP-based LED samples in this work were grown on Si-doped 2° off (100) oriented to (111) GaAs substrates by an Aixtron low pressure metallorganic chemical vapor (MOCVD) deposition system. Trimethyl-gallium, trimethyl-aluminum, and trimethyl-indium were used as the group-III sources. Arsine (AsH_3) and phosphine (PH_3) were the group-V sources. Disilane (Si_2H_6) and bis(cyclopeantadienyl) magnesium (Cp_2Mg) were the n- and p-type doping sources, respectively. In addition, carbon tetrabromide (CBr_4) was used as a second p-type dopant for the contact layer. Hydrogen (H_2) was used as the carrier gas. All of the source materials were of high purity grade. A schematic cross section view of the studied AlGaInP-based LEDs with different contact layers is shown in Fig. 1. Three different samples denoted as devices A, B, and C were presented. The LED structure was composed of a 0.3 μm Si-doped GaAs buffer, a Si-doped distributed Bragg reflector, a 0.75 μm Si-doped AlInP cladding layer ($n = 1 \times 10^{18}$ cm^{-3}), a 20-period [$(Al_{0.2}Ga_{0.8})_{0.5}In_{0.5}P$ 80 Å/$Al_{0.5}In_{0.5}P$ 200 Å] multiple quantum well (MQW) active layer, a 0.75 μm Mg-doped AlInP cladding layer ($p = 4 \times 10^{17}$ cm^{-3}), and a 8 μm Mg-doped GaP window layer. In addition, device B has a C-doped GaP contact layer, while device C has a C-doped GaAs contact layer, both of which are 30 nm thick. Both contact layers were deposited onto the Mg-doped GaP window layer with high carrier concentrations ($p > 1 \times 10^{19}$ cm^{-3}). These C-doped contact layers were grown at a low growth temperature of 530°C with the same V/III ratio of 11. The peak emission wavelength of the studied device was around 630 nm. Clearly, device A was a conventional structure, and the Mg-doped GaP layer was used as the current spreading and metal contact. However, devices B and C, the improved structures, have structures similar to device A except for the use of C-doped GaP and GaAs contact layers. The fabrication processes of these devices were briefly described as follows: First, a 3000 Å ITO was evaporated only on devices B and C. Then, p-type (AuBe) and n-type (AuGeNi) electrodes were deposited separately on all studied devices. Here, different annealing temperatures (300, 400, 500, and 600°C) and times (10, 20, and 30 min) were used to achieve the optimized specific contact resistances of individual devices B and C, as shown in Fig. 2. Obviously, a negligible variation in contact resistance was observed for device C. Yet, device B ex-

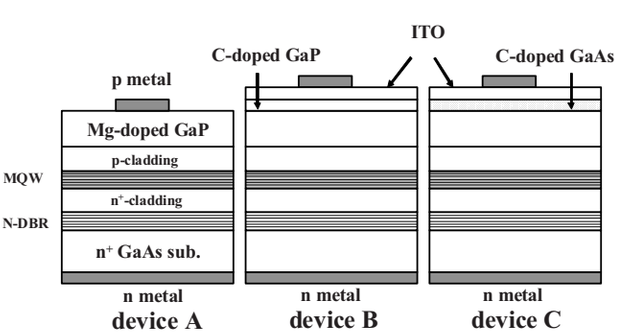

Figure 1. (Color online) Schematic cross sections of the studied AlInP/AlGaInP MQW LEDs.

[z] E-mail: wcliu@mail.ncku.edu.tw

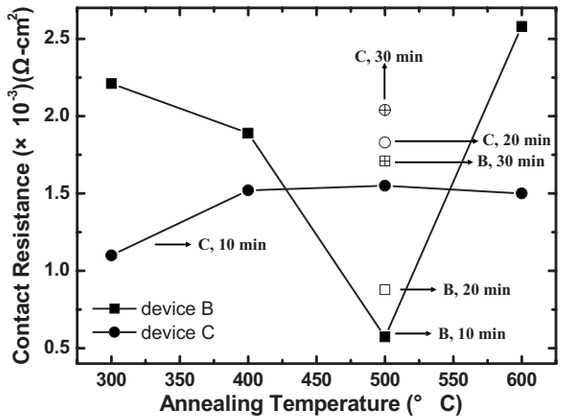

Figure 2. The specific contact resistance as a function of annealing temperature and time.

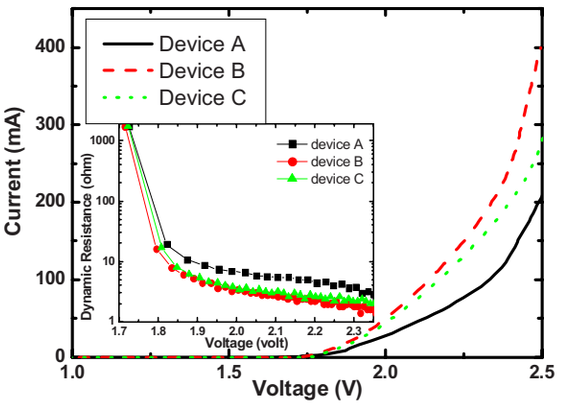

Figure 4. (Color online) Forward *I-V* characteristics of the studied LEDs. The inset shows the dynamic resistances as a function of voltage.

hibited the best contact resistance (5.72×10^{-4} Ω cm^2) at 500°C. This value was significantly lower than the previous paper.[11] The postannealing temperature could not only improve the crystal quality but also further activate doped carbon acceptors in this carbon-doped GaP contact layer. However, the alloyed temperature as high as 600°C and the annealing time longer than 10 min possibly deteriorated the crystallinity of the ITO thin film. This resulted in an increased specific contact resistance of device B. Finally, all devices were annealed in a furnace at 510°C under N_2 ambient for 10 min. The contact properties of studied structures were characterized before the dicing process (280 × 280 μm for individual chips). The chips were attached and bonded to a TO-3 submount for the electrical and optical tests. The current–voltage (*I-V*) curves of studied devices were characterized at room temperature by a semiconductor parameter analyzer (HP 4156). The light output power was measured by a Si photodetector integrated with a current source. The various fabricated LED chips were aged at room temperature under a dc current of 50 mA.

Results and Discussion

Figure 3 shows the contact properties of studied devices. For comparison, device A with an ITO spreading layer inserted between a p-metal and a GaP layer, as shown in the inset, is also included. Clearly, a very poor ohmic contact property to the GaP/ITO interface is observed for device A. This also agrees well with our previous paper.[12] Experimentally, the surface contact resistances are 9.01, 5.62, and 5.92 Ω for devices A, B, and C, respectively. Devices B and C exhibit improved surface contact resistance compared with device A due to the presence of highly C-doped GaP and GaAs layers. In addition, a rather lower surface contact resistance is observed for device B. It is believed that the band discontinuity between the C-doped GaAs contact and the Mg-doped window layers deteriorates the current spreading, thus limiting the contact resistance of LEDs.

Figure 4 shows the forward *I-V* characterizations of devices A, B, and C. The turn-on voltages at 20 mA are 1.95, 1.88, and 1.90 for devices A, B, and C, respectively. For devices B and C, both the improved surface contact properties induced by the C-doped GaP (GaAs) layer as well as the superior current-spreading capability caused by the ITO layer could reduce the series resistances and decrease the turn-on voltages. Furthermore, due to the lattice-matched C-doped GaP contact and the Mg-doped GaP window layer (device B), the lowest turn-on voltage is expected. The inset depicts the dynamic resistances ($\Delta V/\Delta I$) as a function of voltage. Under a 20 mA dc injection current, the dynamic resistances of 7.4, 5.1, and 5.4 Ω are obtained for devices A, B, and C, respectively. The result indicates that the C-doped GaP layer of device B not only improves the contact property, but also reduces the band discontinuity between the conventional C-doped GaAs contact and Mg-doped GaP window layers. Also, these values are lower than the previous paper.[11] Figure 5 shows the whole *I-V* characteristics for all studied devices. Both devices B and C exhibit similar reserve-biased and low current forward-biased behaviors. The transition from a nonra-

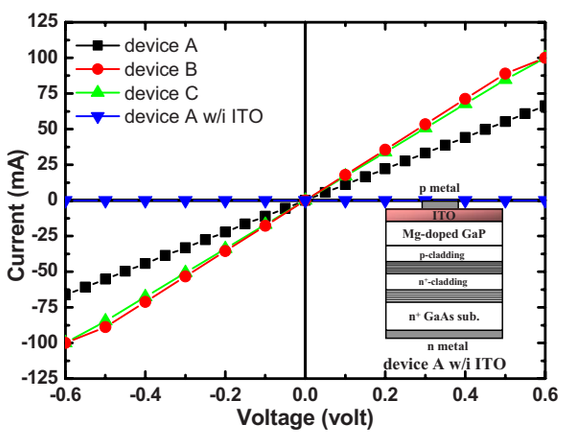

Figure 3. (Color online) Ohmic contact properties of the studied AlInP/AlGaInP MQW LEDs. Device A with an ITO film (shown in the inset) is also included for comparison.

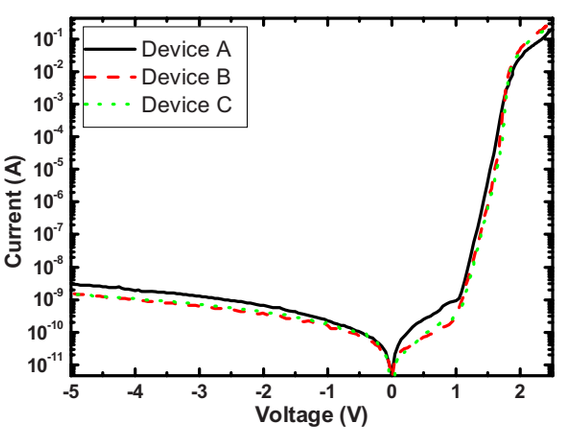

Figure 5. (Color online) *I-V* characteristics of the studied LEDs.

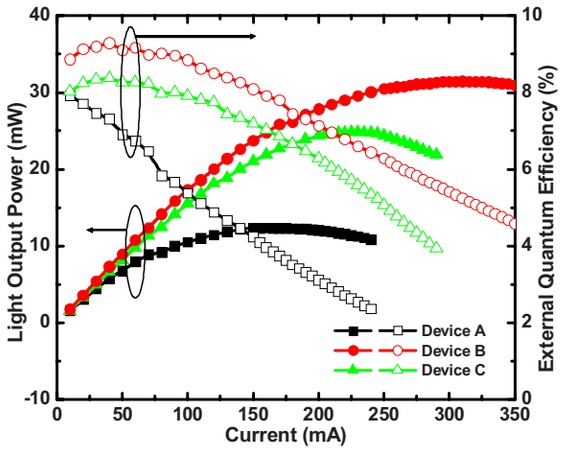

Figure 6. (Color online) Light output power (closed symbols) and EQE (open symbols) vs dc operation current for studied LEDs.

diative recombination injection, which is dominated by surface leakage, to radiative diffusion injection is found at an applied voltage at around 1.7 V. Obviously, these curves show nearly the same ideality factors no matter which contact layer is employed.

The reduced series resistance correlates to the reduction in both junction heating and current crowding effect of an ITO film.[9] Figure 6 shows the light output power and the external quantum efficiency (EQE) as a function of current. Clearly, both the substantial improvements on light output power and EQE are obtained for devices B and C due to the improved turn-on voltage and series resistance characteristics. At room temperature, with increasing the injection current, the light output power of the studied LEDs B and C shows remarkable enhancement over LED A. In addition, the light output power exhibits saturated behaviors in the higher operation current region. For device A, the light output power approaches saturation near 150 mA and then gradually decays. Device B has the higher current operation capability than device C, as confirmed by Fig. 4. This is certainly attributed to the use of C-doped GaP as the surface contact layer between the Mg-doped GaP window layer and the ITO film for device B, as mentioned above. The use of C-doped GaP material (device B) has many advantages, such as better current spreading characteristics, small band discontinuity between the GaP window layer and ITO film, and less optical absorption over the C-doped GaAs material (device C). Hence, the thermal effects resulted from the heterointerface between GaAs and GaP layers can be substantially suppressed for device B. In Fig. 6, the maximum light output powers are 12.4, 31.4, and 24.8 mW at 150, 310, and 225 mA for devices A, B, and C, respectively. These values are approximately 4.1, 8.7, and 7.6 times the light output power at 20 mA. Clearly, the intensity is higher for device B. Device B exhibits the increased light output powers by 92 and 13%, at 150 mA, compared with devices A and C, respectively. Furthermore, under 20 mA, the light output powers are 3.04, 3.60, and 3.26 mW for devices A, B, and C, respectively. Device B shows light output power enhancements by 19 and 11% compared with those of devices A and C. This value is significantly higher than the previous paper.[11] In summary, both under high and low current regions, the light output power is significantly improved by device B. Meanwhile, device B also shows 10–15% improvement on EQE at 20 mA and over 20% enhancement at a higher current region. Although the total light output power of an LED is an important factor, for various applications, the luminescence emitted by an LED should be further considered when a high luminous flux is required. The luminous efficiency of an LED is the ratio between luminous flux and input electric power. The highest luminous efficiency is obtained for a monochromatic emission at 555 nm, at which the human eye is most sensitive. For device B, the luminous efficiency is 19.2 lm/W at 20 mA, which is substantially higher than those of 15.6 and 17.8 lm/W for devices A and C, respectively. Device B exhibits 23.1 and 7.6% improvements on luminous efficiency compared with devices A and C. For device B, the maximum luminescence is 4.72 lm at 250 mA, which is approximately 6.5 times in magnitude than that at 20 mA.

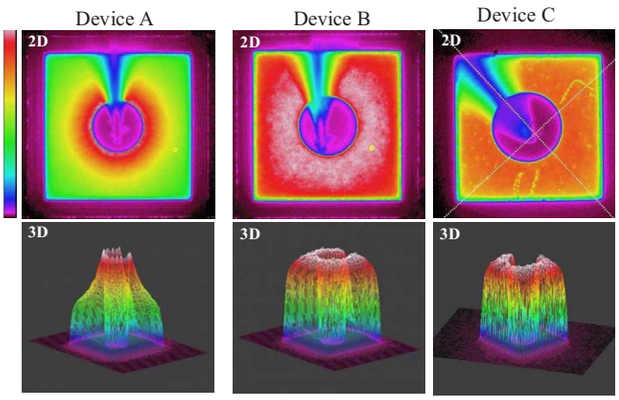

Figure 7. (Color online) Light output power images of studied LEDs.

Figure 7 illustrates the output light images of devices A, B, and C under a 20 mA dc current. Here, both two- and three-dimensional images are shown. The output light intensity and uniformity on the device surface are clearly displayed based on the color bar. From these photographs, a higher EQE could obviously be observed for devices B and C, which indicates that they are superior in current spreading ability compared with device A. The injected current is always crowded nearby the circular p-metal pad, which yields the thermal heating effect for device A. This result agrees well with Fig. 6. In addition, due to the absorption nature as well as the band discontinuity introduced by the C-doped GaAs layer, the efficiency of device C is relatively lower and limited compared with that of device B.

The light emission wavelengths of studied devices are similar, around 620–621 nm under the injection current of 10 mA. Figure 8 shows the emission wavelength, defined as the peak of the electroluminescence (EL) spectrum as a function of an operation current. The wavelength shift for device B is around 1.7 nm from 10 to 200 mA. This value is better than those of 2.4 and 2.1 nm for devices A and C. It could be explained by the fact that the higher concentration of the C-doped GaP layer exhibits a continuous band structure and more uniformity of current spreading. Accordingly, it lowers the junction temperature and results in a smaller wavelength variation.

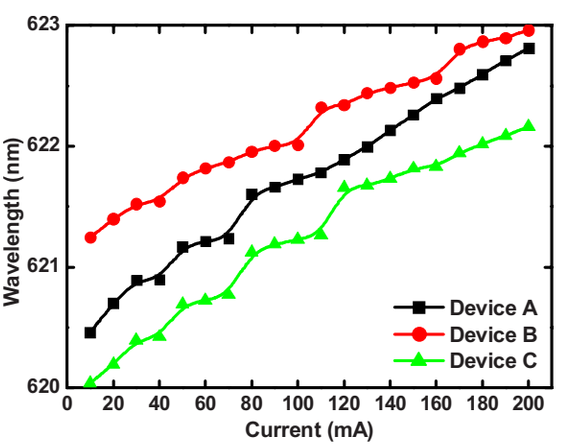

Figure 8. (Color online) The light emission wavelength as a function of dc injection current.

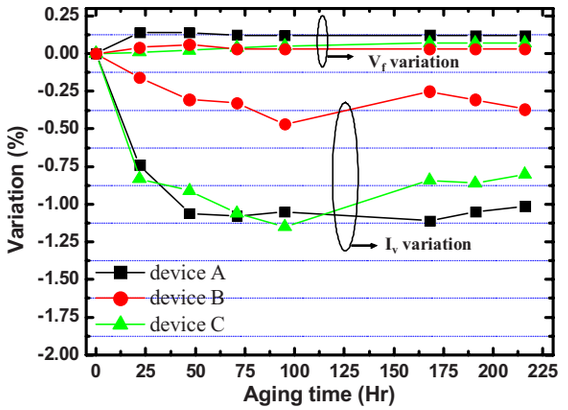

Figure 9. (Color online) Variations in turn-on voltage (V_f) and luminous intensity (I_v) as a function of aging time.

The life test is aged by injecting a 50 mA current into studied LEDs. The variations in the turn-on voltage (V_f) and luminous intensity (I_v) are shown in Fig. 9. Upon aging for 220 h, the I_v degradations are around 1, 0.3, and 0.75% for devices A, B, and C, respectively. The more serious thermal-induced optical deterioration of device A is found due to the larger series resistance and poorer current spreading capability. Because of the Joule heating effect, the device with a higher junction temperature suffers from the structure damage/defect induced by hot carriers.[13] The damage is generated particularly in the heterojunction (e.g., MQW) during aging. Thus, the light behavior is decreased gradually. In addition, the luminous intensity of device B remains at 99.7% of the original value even after 220 h aging time. This is significantly lower than that of device C. Here, the advantage related to the C-doped GaP contact layer over the conventional C-doped GaAs one is apparently presented. The V_f variations between studied devices could be neglected. This is caused by the relatively negligible influence from thermal-induced defects under higher forward current regions.[14] Therefore, based on these results, the C-doped GaP contact layer with ITO film can indeed significantly improve the performance of AlGaInP-based LEDs.

Conclusion

The interesting properties of AlGaInP-based LEDs with/without thin C-doped contact layers, grown by MOCVD, are presented and studied. A substantially higher light output power up to 31.4 mW, at 310 mA, and a higher EQE are obtained in an LED with a C-doped GaP contact layer. This is mainly attributed to the effectively suppressed optical absorption, and the reduced series resistance resulted from the use of a high concentration C-doped GaP contact layer. The significantly lower dynamic resistance of 5.1 Ω, at 20 mA, is attributed to its superior electrical and optical properties. Furthermore, this device also shows the lowest wavelength shift of 1.7 nm, from 10 to 200 mA in the EL spectrum. In addition, the luminous intensity of this device remains at 99.7% of the original value after 220 h aging time. Therefore, the high concentration C-doped GaP contact layer structure provides promise for high performance AlGaInP-based LED applications.

Acknowledgments

The authors thank the National Science Council of Taiwan for financially supporting this research under contract NSC 97-2221-E-006-238-MY3.

National Cheng-Kung University assisted in meeting the publication costs of this article.

References

1. R. M. Lin, J. C. Li, Y. L. Chou, and M. C. Wu, *IEEE Photonics Technol. Lett.*, **18**, 1642 (2006).
2. K. Streubel, N. Linder, R. Wirth, and A. Jaeger, *IEEE J. Sel. Top. Quantum Electron.*, **8**, 321 (2002).
3. J. Y. Su, H. C. Wang, W. B. Chen, S. M. Chen, M. C. Wu, H. H. Chen, and Y. K. Su, *IEEE Trans. Electron Devices*, **50**, 2388 (2003).
4. J. Y. Su, W. B. Chen, M. C. Wu, Y. K. Su, and K. M. Liang, *IEEE Photonics Technol. Lett.*, **16**, 30 (2004).
5. H. Sugawara, M. Ishikawa, and G. Hatakoshi, *Appl. Phys. Lett.*, **58**, 1010 (1991).
6. S. C. Hsu, D. S. Wuu, X. Zheng, and R. H. Horng, *J. Electrochem. Soc.*, **156**, H281 (2009).
7. R. M. Perks, J. Kettle, A. Porch, and D. V. Morgan, *Thin Solid Films*, **515**, 8660 (2007).
8. J. F. Lin, M. C. Wu, M. J. Jou, C. M. Chang, B. J. Lee, and Y. T. Tsai, *Electron. Lett.*, **30**, 1793 (1994).
9. G. B. Stringfellow and M. G. Craford, *Semicond. Semimetals*, **48**, 1 (1997).
10. C. H. Yen, Y. J. Liu, N. Y. Huang, K. H. Yu, T. P. Chen, L. Y. Chen, T. H. Tsai, C. Y. Lee, and W. C. Liu, *IEEE Photonics Technol. Lett.*, **20**, 1923 (2008).
11. S. C. Hsu, D. S. Wuu, X. Zheng, R. H. Horng, and J. Y. Su, *Jpn. J. Appl. Phys.*, **47**, 7023 (2008).
12. C. H. Yen, Y. J. Liu, K. K. Yu, P. L. Lin, T. P. Chen, L. Y. Chen, T. H. Tsai, and W. C. Liu, *IEEE Electron Device Lett.*, **30**, 359 (2009).
13. M. Meneghini, L. R. Trevisanello, G. Meneghesso, and E. Zanoni, *IEEE Trans. Device Mater. Reliab.*, **8**, 323 (2008).
14. O. Pursiainen, N. Linder, A. Jaeger, R. Oberschmid, and K. Streubel, *Appl. Phys. Lett.*, **79**, 2895 (2001).